Image Segmentation using Gradient-based Histogram Thresholding for Skin Lesion Delineation

Pedro M. M. Pereira[1,3], Luis M. N. Tavora[2], Rui Fonseca-Pinto[2], Rui Pedro Paiva[3,4],
Pedro A. A. Assuncao[1,2] and Sergio M. M. de Faria[1,2]

[1]*Instituto de Telecomunicações, Portugal*
[2]*ESTG, Polytechnic Institute of Leiria, Portugal*
[3]*DEI - FCTUC, University of Coimbra, Portugal*
[4]*CISUC, Department of Informatics Engineering, University of Coimbra, Portugal*

Keywords: Segmentation, Skin Lesion Detection, Medical Imaging, Dermoscopy.

Abstract: Image segmentation is a key stage in medical image processing algorithms and machine learning classifiers where identification of discriminative features are of utmost importance. In the case of skin lesions, most of the existing image segmentation approaches aim at minimising some error metric between computed and ground-truth regions of interest (ROI) defined by medical experts, where ROI delineation is not always considered. This paper proposes an image segmentation method for skin lesion delineation, which expands traditional histogram and clustering-based approaches to achieve the best trade-off between both. The proposed method is capable of providing accurate details of the skin lesion borders, without deviating from the coarser borders of the available ground-truth.

1 INTRODUCTION

In general, medical image processing systems include a segmentation stage to identify regions of interest (ROI) for further processing, which may include texture and colour analysis, feature extraction, etc. In the case of pigmented skin lesions, due to the rather limited human capability to discriminate slight variations in contrast and blur, precise identification of relevant ROI boundaries poses a problem to dermatologists (Claridge and Orun, 2002). Morphological aspects of skin lesions alongside with the large number of environment-variables (e.g. location in the body, skin properties, lighting conditions and angle of view) further increase the challenge of accurate segmentation of the most useful ROI (Celebi et al., 2009a). This results in significant inter and intra-observer variability and coarse ROI segmentation. Thus, to reduce the dependence of human factors, different types of computational methods have been used for image segmentation, spanning over a quite considerable range of categories (Pathan et al., 2018).

Recent advances in machine learning approaches are rapidly changing the landscape of medical image processing algorithms for detection, recognition and classification, where data sets with accurate ground-truth image segmentation are increasingly necessary both for training and validation of such new computational models (Ker et al., 2018; Oliveira et al., 2018). In the case of skin lesion segmentation, the difficulty of achieving accurate delineation of ROI borders manually, has driven research efforts to increase the availability of ground-truth ROI through computational methods (Cheng et al., 2015; Kéchichian et al., 2014). Particularly relevant in the application scope of this work is the mobile system designed for early detection of melanoma recently proposed in (Do et al., 2018), which combines fast segmentation, feature extraction and classification in resource constrained devices.

This paper proposes an accurate segmentation method for pigmented skin lesions, envisaging delineation of melanoma as the main application. In general this kind of medical images produce bi-modal histograms, and although this characteristic has been used as the basis of different segmentation methods, it results in either coarse borders or simply fails to provide significant ROI in images with low colour contrast and smooth texture transitions. Therefore, this work addresses the problem of accurate identification of the relevant ROI in such images, which includes the ability to define the external border of the lesion with

84

high level of precision. Taking into account the clinical relevance of this aspect, a gradient-based metric is devised to drive the proposed delineation method across a refinement histogram-based segmentation algorithm. Two different types of medical images are targeted, which increases the challenge of achieving efficient segmentation with accurate border details in both cases, as pointed out in (Zhou et al., 2008). For this purpose, the Dermofit dataset of macroscopic images (Ballerini et al., 2013) and the PH^2 dataset of dermoscopic images (Mendonça et al., 2013) are both used in this work.

This work is organised as follows: Section 2 presents the background that is relevant for the proposed method. Section 3 describes the Gradient-based metric and Section 4 introduces the proposed method. In Section 5 the obtained experimental results are presented, alongside with the associated discussion. Finally, in Section 6 some conclusions and future work perspectives are presented.

2 SKIN LESION SEGMENTATION - BACKGROUND

As mentioned above, images of skin lesions exhibit two distinctive regions which are associated, one to the lesion itself, and another to the surrounding skin. This leads to bi-modal histograms, as shown in Fig. 1, for images of skin lesions with quite different characteristics. This results not only from the lesion morphology, but also from the use of different image acquisition technologies and lighting conditions. For instance, while accurate segmentation of the skin lesion shown in Fig. 1a is quite easy to be obtained directly from its well-defined histogram, in the case of Fig. 1c it poses a problem due to the blurry borders and low colour contrast. This can be confirmed by the corresponding histogram shown on the right side of Fig. 1, where the pixels belonging to the relevant ROI are quite difficult to identify.

2.1 Histogram Thresholding

Histogram thresholding techniques have long been used for segmentation of these type of images, where the region of the lesion can be distinguished by its different tonality (Korotkov and Garcia, 2012). The underlying idea of these methods is to perform a binary partition of the image based on the luminance level of each pixel, meaning in this case (e.g. Fig. 1) to successfully separate the region of the lesion (darker region $\leftrightarrow$ left Y-peak: Y_{Pmin}) from the surrounding skin (right Y-peak: Y_{Pmax}). In a simple formulation,

the segmentation challenge to be considered here is to find an optimum criterion to define a threshold value (Y_{th}) that leads to an accurate ROI extraction, i.e., the region of the image that contains the lesion. Different threshold techniques exist for decades (Sahoo et al., 1988), and this operation can be done either directly on the Y-histogram or after a transformation $T(Y)$, as proposed in (Rajab et al., 2004). Nevertheless, the performance of the method might strongly depend on the distribution of luminance values, as inferred from Fig. 1c and even Fig. 1b.

2.2 Clustering

Clustering algorithms have also been used for skin lesion segmentation based on different approaches (Melli et al., 2006; Tasoulis et al., 2010; Iyatomi et al., 2008; Ganster et al., 2001). The algorithms can be fed with image information in different formats such as *RGB*, *YUV* or *YCbCr*, but there are also systems using only the luminance Y channel since the inherent fusion process of the *RGB* channels allows inclusion of the relevant colour information (Maglogiannis and Doukas, 2009). A quite efficient clustering approach is based on the so called *K-Means*, or Lloyd's algorithm (Lloyd, 1982), which is an iterative data-partitioning algorithm that assigns, for a predefined number of clusters, every input observation to only one of the clusters. In skin lesion images, clustering algorithms may take advantage of the bi-modal characteristics of the histogram to use the corresponding peaks as the initial centroids.

2.3 Other Approaches

Several other segmentation approaches are worthwhile to be mentioned. For instance, the concept of *Fuzzy Differential Evolution Entropy* (FT) was used in (Sarkar et al., 2014), through an algorithm that creates fuzzy partitions from the image histogram. Then the entropy is optimised to obtain the thresholds using a differential evolution meta-heuristic. Another algorithm based on a similar approach is the *Fuzzy Clustering LevelSet* (FL) (Li et al., 2011), which uses a hybrid model that alternates between global and local region competitions using spatial information in the fuzzy clustering technique. For Quantization approaches one can find early methods based on *PCT (Principal Components Transform) Median Cut* (PM) (Umbaugh et al., 1993), while Active Contours were proposed in (Chan et al., 2000) and (Lankton and Tannenbaum, 2008), referred as *Chan-Vese* (CV) and *Lankton Mean Separation* (LM). In the former a Mumford-Shah function is minimised over the length
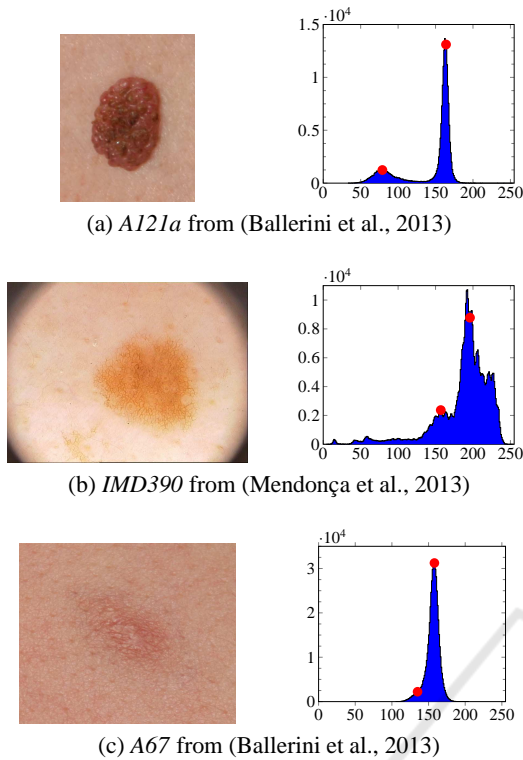
(a) *A121a* from (Ballerini et al., 2013)

(b) *IMD390* from (Mendonça et al., 2013)

(c) *A67* from (Ballerini et al., 2013)

Figure 1: Skin lesion images (left) and the corresponding luminance (Y) histograms (right), were red dots represent peaks that correspond to the lesion and skin, respectively.

of the contour, while the latter uses local image statistics and evolving contours based on local information. Additionally, traditional methods like *Otsu Threshold* (OT) (Otsu, 1979) and *K-Means Colour* (KC) (Melli et al., 2006) also serve as baseline literature.

3 GRADIENT-BASED METRIC

The figure of merit that is herein proposed to assess the accuracy of a given outside border line is based on the rationale that the segmentation contour separates regions with substantially different tonalities. Accordingly, the magnitude of the image gradient on contour pixels is expected to yield higher values than in other regions (i.e., either inside the lesion or in the remaining skin). Following this argument, segmentation masks whose border lines exhibit higher gradient magnitudes should more faithfully separate the two regions of the image.

For a given image I, the gradient magnitude in each pixel can be determined by Eq.(1),

$$\left| \vec{G}_j \right| = \left[\left(\frac{\partial I_j}{\partial x} \right)^2 + \left(\frac{\partial I_j}{\partial y} \right)^2 \right]^{1/2}, \tag{1}$$
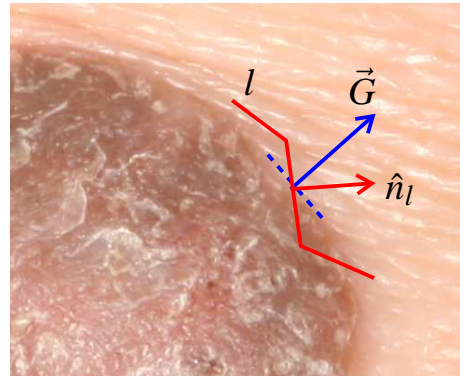
Figure 2: Segmentation border line (red) and gradient: the higher the projection of the image gradient $\vec{G}$ onto $\hat{n}_l$, the more accurate is the border line (Image *P348a* from (Ballerini et al., 2013)).

where j denotes the colour (or luminance) channel under consideration (e.g., $j = R, G, B, Y$). For any point of a border line defined by segmentation, the projection of the gradient vector $\vec{G}$ onto the orthogonal direction of the line ($\hat{n}_l$), defines an accuracy metric for the border line. Such projection is given by (2).

$$G_{\perp l,j} = \vec{G}_{l,j} \cdot \hat{n}_l \tag{2}$$

This concept is depicted in Fig. 2, where one can observe that the orthogonal direction of the segmentation border line (red) is not aligned with the gradient at the same point. The higher the projection $G_{\perp l,j}$ computed by (2) the better (i.e. more accurate) is the lesion contour segment.

Therefore, following the above discussion, the average value of $G_{\perp l,j}$ over all points of a contour line l is used as the gradient-based metric to evaluate how accurately a given segmentation contour represents the outside border on a skin lesion.

4 PROPOSED METHOD

The image segmentation method proposed for skin lesion delineation follows the processing chain depicted in Fig. 3. The underlying idea is to find an optimal ROI delineation based on a trade-off between an ROI with the highest gradient magnitude in the orthogonal direction of its border line, and another ROI with larger area but lower gradient. While the former identifies the sharpest boundary of the skin lesion, the latter contains more boundary information which is also useful for medical analysis and monitoring of temporal evolution. As described next, gradient-based histogram thresholding and clustering are used to generate the two ROIs for final optimisation and delineation of skin lesions.

4.1 Histogram Thresholding

The bi-modal characteristic of skin lesion image histograms is used to determine the two most important peaks, which in turn define the range limits Y_{Pmin}, Y_{Pmax} for all possible thresholds, i.e., the best ROI must be found by cutting the histogram at the optimum threshold $Y_{th*} \in \{Y_{Pmin}, Y_{Pmax}\}$ to be found between the two peaks (e.g. red markers on the histograms of Fig. 1). In the method shown in Fig. 3, histogram thresholding is performed for all values between Y_{Pmin} and Y_{Pmax}, generating an equal number of images and the corresponding segmentation masks. After a filtering process to remove small isolated regions and outliers, a clean ROI is determined for each image and the average gradient $G_\perp$ is computed, as defined by (2). Then the ROI whose border yields the maximum average gradient is selected along with its histogram threshold. In summary, this process ensures that the border line of such ROI is the one with the highest tonality variations across it. In the remaining sections, the ROI obtained by maximising the gradient border through histogram thresholding is identified by HT.

4.2 Clustering

In the proposed method, clustering is used to identify a coarse ROI for the skin lesion where the boundaries include, in general, the smooth transition regions between the lesion and the surrounding healthy skin. In this work the variant *K-Means++* was selected, due to its faster clustering convergence and also good discriminative performance due different heuristics used for finding centroids (Arthur and Vassilvitskii, 2007). The iterative clustering process is carried out with a maximum of 200 iterations seeking for two clusters with a global minimum of the *Euclidean* distance to cluster-centre. For the sake of reproducibility, the initial centroids are defined as the histogram peaks. In the remaining sections, the ROI obtained through clustering is identified by *KM*.

4.3 Filtering

Due to noise, inherent illumination variations and other factors, both the histogram thresholding and clustering methods described above produce ROIs with binary masks that include not only a large blob (the skin lesion region) but also other small isolated regions spread across the whole image. The filtering process devised to remove such unwanted regions assumes that the lesion region limits are fully located within the image, so the first operation is to remove all isolated regions with any boundary coincident with the image borders. This is done by using a flood-fill algorithm based on morphological reconstruction (Soille, 2013). This first cleansing operation is especially relevant when processing images from the PH^2 dataset, as they exhibit a black circular frame artificially introduced in the dermatoscope digitisation process. The relevant ROI containing the lesion is then determined by extracting the blob with the largest area in the binary mask, using a labelling procedure (Haralick and Shapiro, 1992, p. 40-48).

4.4 Optimised Segmentation

The optimisation step aims at improving delineation of skin lesions by selectively expanding the ROI border that was previously found through histogram thresholding with gradient maximisation, in order to further include relevant areas of transition regions. This is necessary because gradient maximisation often leads to stringent contour lines which only include the inner parts of the lesion and leave out relevant transition regions. Taking into account that clustering-based segmentation usually results in the inclusion of a larger region around the inner part of the lesion, the proposed optimisation procedure achieves the best trade-off between gradient maximisation and increased ROI area to include transition regions. This is done by finding an optimum threshold (Y_{th*}) that maximises, simultaneously, both the gradient of the border line $G_\perp$ and the ROI area.

For each ROI obtained through histogram thresholding (HT) and clustering (KM), as described above, let us define the following reference values:

- $G_{\perp,KM}$ and $G_{\perp,HT}$: the average gradient of the border (in (2));

- A_{KM} and A_{HT}: the area of the ROI, i.e. skin lesion.

The corresponding values associated to an arbitrary histogram threshold Y_{th} are defined as $G_{\perp,Y_{th}}$ and $A_{Y_{th}}$, respectively. The ratios $R_G(Y_{th})$ and $R_A(Y_{th})$ (expression (3)) define the relative gradient and relative area of any ROI obtained with threshold Y_{th}, using the HT and KM ROIs as references.

$$R_G(Y_{th}) = \frac{G_{\perp,Y_{th}}}{G_{\perp,KM}} \quad R_A(Y_{th}) = \frac{A_{Y_{th}}}{min(A_{KM}, A_{HT})} \quad (3)$$

The optimisation procedure consists in finding the optimum threshold Y_{th*} that maximises both $R_G(Y_{th})$ and $R_A(Y_{th})$. This is accomplished by maximising their product, provided that the selected maximum does not lead to gradient values below that of the KM ROI ($G_{\perp,KM}$) and the new ROI area falls between
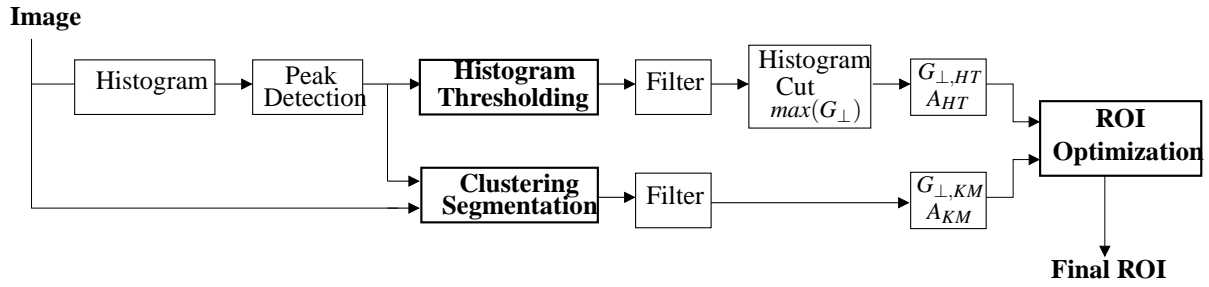
Image

Figure 3: Proposed scheme.

those of *HT* and *KM* ROIs. This is equivalent to solve the following constrained maximisation problem:

$$Y_{th^*} = \arg\max_{Y_{th} \in Y} R_G(Y_{th}) R_A(Y_{th}) \tag{4}$$

subject to:

$$R_G \geq 1 \wedge R_A \geq 1 \wedge \frac{A_{Y_{th}}}{max(A_{KM}, A_{HT})} \leq 1 \tag{5}$$

In summary, the optimal histogram threshold Y_{th^*} to be used for delineation of skin lesions is found through a trade-off between border gradient and amount of transition area included in the ROI.

5 EXPERIMENTAL RESULTS AND DISCUSSION

The performance of the segmentation algorithm described in Section 4 was evaluated using sets of images from different databases. A total of 195 images from the Dermofit dataset (Ballerini et al., 2013) and 32 images from the PH^2 dataset (Mendonça et al., 2013) were used. This selection followed two main criteria: *i*) images without hair strands crossing the lesion, i.e., as hairless as possible and *ii*) lesion limits within the image, i.e., the whole lesion boundary fully located inside the image.

In the first stage the input grayscale image passes through two segmentation processes, namely Histogram Thresholding and Clustering Segmentation. As pointed out in section 4, the output of both algorithms may exhibit some image artefacts, which can be observed in Fig. 4b and Fig. 4e. Then the efficiency of the filtering stage, that is used after both segmentation algorithms (described in Section 4.3), in removing the small isolated regions, is shown in Fig. 4c and Fig. 4f. In these images it is possible to observe that the filtering process is quite effective in providing an accurate lesion/skin segmentation mask without harming the border details.

After the segmentation and filtering stages, accurate ROI delineation is performed, following the optimisation procedure described in the previous section.

(a) Image *B964*   (b) Histogram TH   (c) Filtered

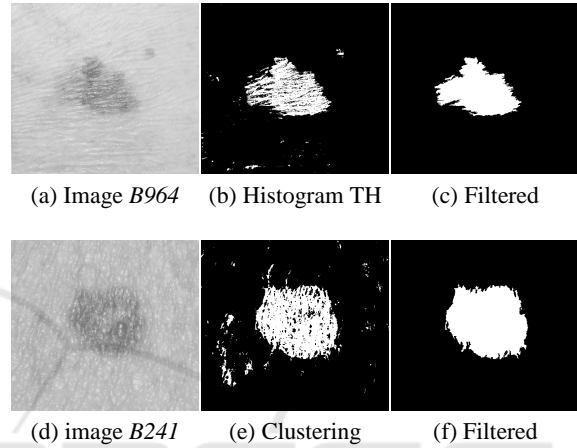(d) image *B241*   (e) Clustering   (f) Filtered

Figure 4: Image segmentation using *Histogram thresholding (HT)* and *K-Means (KM)* clustering: (a,d) original grayscale images from (Ballerini et al., 2013), (b,e) segmentation output, (c,f) final binary mask after the filtering operation.

For visual evaluation and discussion, a set of representative types of skin lesions have been selected from the datasets to represent the segmentation results, which is depicted in Fig. 5.

In Fig. 5 the lesion segmentation using *KM* is represented by a red line, the *HT* by a green line and the *Proposed* method by a blue line. The white line represents the ground-truth (GT) provided by the dataset.

From the representative results presented in Fig. 5a to Fig. 5e, it can be observed that the algorithms are in general quite effective in the segmentation of images and delineation of the relevant ROI.

The Histogram Thresholding method (*HT*) is able to achieve accurate delineation when there is a sharp tonality difference between the skin lesion and the surrounding skin. However, as mentioned before, in images with smoother lesion-to-skin transitions, the highest value of $G_\perp$, may result in a segmented region that is smaller than expected. This effect can be seen in images from Fig. 5f to Fig. 5l. This kind of output is not the most useful from the clinical point of view, as it may exclude a relevant part of the lesion.

In the case of Clustering ROI segmentation (*KM*),

(a) *D427b* (b) *D155b* (c) *B447a*

(d) *D384* (e) *A121a* (f) *B311c*

(g) *A92* (h) *B17a* (i) *B964*
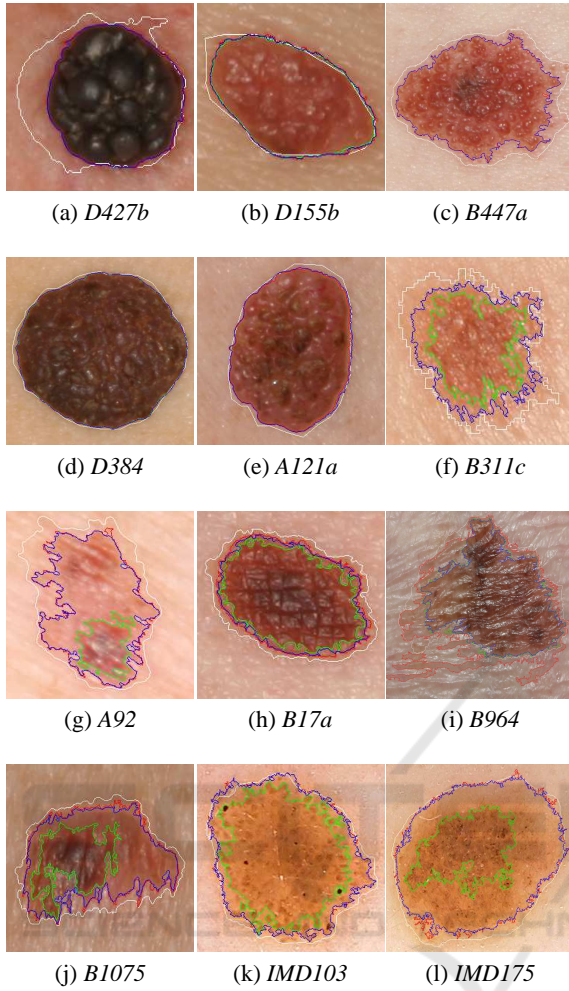
(j) *B1075* (k) *IMD103* (l) *IMD175*

Figure 5: Skin lesion segmentation using *KM* (red), *HT* (green) and *Proposed* (blue). The white line corresponds to the dataset provided ground-truth (GT). Images (a) to (j) are from (Ballerini et al., 2013), and (k) and (l) from (Mendonça et al., 2013).

in general, the segmented region may include smooth transition regions between the lesion and the surrounding healthy skin. This commonly results in a larger region than that obtained by the Histogram Threshold method, as can be seen in images Fig. 5h, Fig. 5i, Fig. 5j and Fig. 5l. In such cases, this might not represent the best option as well.

In order to overcome the *HT* underestimation of the ROI and the possible *KM* overestimation, the proposed combined method relies on a trade-off between the ROI and the border gradient. As can be observed in all images of Fig. 5, the blue line always represents a more precise delineation of the ROI.

Some authors compare the segmentation results with the ground-truth (GT) segmentation masks provided in the databases. Nevertheless, as can be visu-

ally observed in Fig. 5a, Fig. 5b and Fig. 5f, the GT borders are not as accurate and spatially detailed as those obtained with the used algorithms. It can also be observed that the GT lines often miss areas with high texture variations.

In numerical terms, other performance indicators are usually considered as benchmarks (Hance et al., 1996; Celebi et al., 2009b; Garnavi et al., 2011):

- Border Error (BE), in (6), a measure of the fraction of non-overlapping (exclusive-OR, $\oplus$) segmentation regions (Area) between the proposed segmentation (PS) method and the dataset ground-truth segmentation (GT);

$$\text{BE}(PS, GT) = \frac{\text{Area}(PS \oplus GT)}{\text{Area}(GT)} \quad (6)$$

- True Detection Rate (TDR), in (7), an indicator of the ratio of number of pixels (np) that are correctly classified as lesion;

$$\text{TDR}(PS, GT) = \frac{np(PS \cap GT)}{np(GT)} \quad (7)$$

- False Positive Rate (FPR), in (8), which accounts for the number of pixels that are incorrectly classified as lesion.

$$\text{FPR}(PS, GT) = \frac{np(PS \cap \overline{GT})}{np(GT)} \quad (8)$$

The results obtained for these indicators are presented in Table 1, alongside with those from the methods presented in Section 2.3. It can been seen that the performance of the proposed algorithm (*Prop*) is generally inline with others published in the literature, though not always consistent for all metrics. However, it should be kept in mind that these indicators use the GT as reference, which does not provide segmentation masks with as much spatial details as those herein obtained. Such difference can be clearly observed in Fig. 5

The gradient metric defined in Section 3 was also used to assess the performance of the proposed method. The quotient of gradient between delineations for both datasets was determined for such purpose and the results are presented in Table 2. Observing its first three lines, it can be seen that *HT* has on average the highest $G_\perp$ values, as the method was optimised for such purpose, though in some cases this also corresponds to inaccurate segmentation. The second group of three lines make it clear that the *Prop* method outperforms *KM* while only slightly compromising the $G_\perp$ value in comparison with the maximum of *HT*. The remaining data on the table also shows that the *Prop* method produces segmentations

Table 1: Ground Truth (GT)-based indicators (%).

Method	Dermofit			PH2		
	BE	TDR	FPR	BE	TDR	FPR
OT	32.569	76.386	7.483	20.907	83.999	7.061
KC	53.475	78.439	8.581	18.174	86.041	6.313
FT	1.017	37.819	25.731	50.499	50.734	15.319
FL	2.439	49.500	50.084	20.352	82.846	6.872
PM	1.504	97.456	23.096	1.107	93.442	24.524
CV	2.383	69.381	35.618	48.521	68.161	14.119
LM	2.164	0.0003	52.467	1.604	94.543	36.550
HT	36.253	64.920	9.409	34.763	65.586	11.165
KM	21.592	79.336	5.554	17.732	85.113	6.085
Prop	23.034	78.283	6.008	20.336	81.676	6.950

with $G_\perp$ values higher than any of the other algorithms previously introduced. This means that skin lesion delineation obtained by the proposed method is more accurate than the others because the border line is found where the gradient is higher, i.e., a better discrimination between lesion and normal skin is obtained.

Table 2: Average Border Gradient indicators.

Indicators	Dermofit	PH2
$G_{\perp,HT}$ / $G_{\perp,KM}$	1.173	1.271
$G_{\perp,Prop}$ / $G_{\perp,HT}$	0.933	0.917
$G_{\perp,Prop}$ / $G_{\perp,KM}$	1.082	1.086
$G_{\perp,HT}$ / $G_{\perp,GT}$	3.908	4.742
$G_{\perp,KM}$ / $G_{\perp,GT}$	3.364	3.997
$G_{\perp,Prop}$ / $G_{\perp,GT}$	3.688	4.301
$G_{\perp,Prop}$ / $G_{\perp,OT}$	1,831	1,916
$G_{\perp,Prop}$ / $G_{\perp,KC}$	1,831	1,921
$G_{\perp,Prop}$ / $G_{\perp,FT}$	2,268	1,787
$G_{\perp,Prop}$ / $G_{\perp,FL}$	6,429	1,829
$G_{\perp,Prop}$ / $G_{\perp,PM}$	2,894	2,701
$G_{\perp,Prop}$ / $G_{\perp,CV}$	1,175	1,086
$G_{\perp,Prop}$ / $G_{\perp,LM}$	3,376	3,191

6 CONCLUSIONS

This paper addressed the segmentation of skin lesion images using both histogram thresholding and clustering algorithms to overcome the limitations of each one on its own. A gradient-based method was devised for optimised thresholding and ROI border quality parameter. The segmentation masks obtained for the final ROIs indicate that this method is quite accurate in delineation of the relevant lesion regions containing for a wide range of images. The experimental validation, using two publicly available images datasets, show that the proposed approach is effective in delineating skin lesions with detailed geometry in regions with quite diverse tonality variations. The accurate delineation of skin lesions is a relevant achievement to provide discriminative features for machine learning algorithms and also to investigate patterns of temporal evolution of the borders.

ACKNOWLEDGEMENTS

REFERENCES

Arthur, D. and Vassilvitskii, S. (2007). k-means++: The advantages of careful seeding. In *Proceedings of the eighteenth annual ACM-SIAM symposium on Discrete algorithms*, pages 1027–1035. Society for Industrial and Applied Mathematics.

Ballerini, L., Fisher, R. B., Aldridge, B., and Rees, J. (2013). A color and texture based hierarchical k-nn approach to the classification of non-melanoma skin lesions. In *Color Medical Image Analysis*, pages 63–86. Springer. https://licensing.edinburgh-innovations.ed.ac.uk/i/software/dermofit-image-library.html.

Celebi, M. E., Iyatomi, H., Schaefer, G., and Stoecker, W. V. (2009a). Lesion border detection in dermoscopy images. *Computerized medical imaging and graphics*, 33(2):148–153.

Celebi, M. E., Schaefer, G., Iyatomi, H., Stoecker, W. V., Malters, J. M., and Grichnik, J. M. (2009b). An improved objective evaluation measure for border detection in dermoscopy images. *Skin Research and Technology*, 15(4):444–450.

Chan, T. F., Sandberg, B. Y., and Vese, L. A. (2000). Active contours without edges for vector-valued images. *Journal of Visual Communication and Image Representation*, 11(2):130–141.

Cheng, I., Sun, X., Alsufyani, N., Xiong, Z., Major, P., and Basu, A. (2015). Ground truth delineation for medical image segmentation based on local consistency and distribution map analysis. In *37th Annual International Conference of the IEEE Engineering in Medicine and Biology Society (EMBC)*, pages 3073–3076.

Claridge, E. and Orun, A. (2002). Modelling of edge profiles in pigmented skin lesions. In *Proceedings of medical image understanding and analysis*, pages 53–56.

Do, T. T., Hoang, T., Pomponiu, V., Zhou, Y., Zhao, C., Cheung, N. M., Koh, D., Tan, A., and Hoon, T. (2018). Accessible melanoma detection using smartphones and mobile image analysis. *IEEE Transactions on Multimedia*, pages 1–1.

Ganster, H., Pinz, P., Rohrer, R., Wildling, E., Binder, M., and Kittler, H. (2001). Automated melanoma recognition. *IEEE transactions on medical imaging*, 20(3):233–239.

Garnavi, R., Aldeen, M., and Celebi, M. (2011). Weighted performance index for objective evaluation of border detection methods in dermoscopy images. *Skin Research and Technology*, 17(1):35–44.

Hance, G. A., Umbaugh, S. E., Moss, R. H., and Stoecker, W. V. (1996). Unsupervised color image segmentation: with application to skin tumor borders. *IEEE Engineering in Medicine and Biology Magazine*, 15(1):104–111.

Haralick, R. M. and Shapiro, L. G. (1992). *Computer and robot vision*. Addison-wesley.

Iyatomi, H., Oka, H., Celebi, M. E., Hashimoto, M., Hagiwara, M., Tanaka, M., and Ogawa, K. (2008). An improved internet-based melanoma screening system with dermatologist-like tumor area extraction algorithm. *Computerized Medical Imaging and Graphics*, 32(7):566–579.

Kéchichian, R., Gong, H., Revenu, M., Lezoray, O., and Desvignes, M. (2014). New data model for graph-cut segmentation: Application to automatic melanoma delineation. In *2014 IEEE International Conference on Image Processing (ICIP)*, pages 892–896.

Ker, J., Wang, L., Rao, J., and Lim, T. (2018). Deep learning applications in medical image analysis. *IEEE Access*, 6:9375–9389.

Korotkov, K. and Garcia, R. (2012). Computerized analysis of pigmented skin lesions: A review. *Artificial intelligence in medicine*, 56(2):69–90.

Lankton, S. and Tannenbaum, A. (2008). Localizing region-based active contours. *IEEE transactions on image processing*, 17(11):2029–2039.

Li, B. N., Chui, C. K., Chang, S., and Ong, S. H. (2011). Integrating spatial fuzzy clustering with level set methods for automated medical image segmentation. *Computers in biology and medicine*, 41(1):1–10.

Lloyd, S. (1982). Least squares quantization in pcm. *IEEE transactions on information theory*, 28(2):129–137.

Maglogiannis, I. and Doukas, C. N. (2009). Overview of advanced computer vision systems for skin lesions characterization. *IEEE transactions on information technology in biomedicine*, 13(5):721–733.

Melli, R., Grana, C., and Cucchiara, R. (2006). Comparison of color clustering algorithms for segmentation of dermatological images. In *Medical Imaging 2006: Image Processing*, volume 6144, page 61443S. International Society for Optics and Photonics.

Mendonça, T., Ferreira, P. M., Marques, J. S., Marcal, A. R., and Rozeira, J. (2013). Ph2-a dermoscopic image database for research and benchmarking. In *Engineering in Medicine and Biology Society (EMBC), 2013 35th Annual International Conference of the IEEE*, pages 5437–5440. IEEE. http://www.fc.up.pt/addi/ph2%20database.html.

Oliveira, R. B., Papa, J. P., Pereira, A. S., and Tavares, J. M. R. (2018). Computational methods for pigmented skin lesion classification in images: review and future trends. *Neural Computing and Applications*, 29(3):613–636.

Otsu, N. (1979). A threshold selection method from gray-level histograms. *IEEE transactions on systems, man, and cybernetics*, 9(1):62–66.

Pathan, S., Prabhu, K. G., and Siddalingaswamy, P. (2018). Techniques and algorithms for computer aided diagnosis of pigmented skin lesions – a review. *Biomedical Signal Processing and Control*, 39:237–262.

Rajab, M., Woolfson, M., and Morgan, S. (2004). Application of region-based segmentation and neural network edge detection to skin lesions. *Computerized Medical Imaging and Graphics*, 28(1):61–68.

Sahoo, P. K., Soltani, S., and Wong, A. K. (1988). A survey of thresholding techniques. *Computer vision, graphics, and image processing*, 41(2):233–260.

Sarkar, S., Paul, S., Burman, R., Das, S., and Chaudhuri, S. S. (2014). A fuzzy entropy based multi-level image thresholding using differential evolution. In *International Conference on Swarm, Evolutionary, and Memetic Computing*, pages 386–395. Springer.

Soille, P. (2013). *Morphological image analysis: principles and applications*. Springer Science & Business Media.

Tasoulis, S., Doukas, C., Maglogiannis, I., and Plagianakos, V. (2010). Classification of dermatological images using advanced clustering techniques. In *Engineering in Medicine and Biology Society (EMBC), 2010 Annual International Conference of the IEEE*, pages 6721–6724. IEEE.

Umbaugh, S. E., Moss, R. H., Stoecker, W. V., and Hance, G. A. (1993). Automatic color segmentation algorithms-with application to skin tumor feature identification. *IEEE Engineering in Medicine and Biology Magazine*, 12(3):75–82.

Zhou, H., Chen, M., Zou, L., Gass, R., Ferris, L., Drogowski, L., and Rehg, J. M. (2008). Spatially constrained segmentation of dermoscopy images. In *Biomedical Imaging: From Nano to Macro, 2008. ISBI 2008. 5th IEEE International Symposium on*, pages 800–803. IEEE.